

# Design of building structure health monitoring model based on IoT and MEMS sensors

Xianrui Song\*

Department of management engineering, Henan Technical College of Construction, Zhengzhou 450000, China

Received: 15 October 2024 / Accepted: 21 August 2025

**Abstract.** Traditional structural health monitoring methods often rely on manual inspection, which is not only inefficient but also suffers from data collection delays, subjective error sensitivity, and the inability to continuously track subtle structural changes in complex buildings over time. Therefore, this study innovatively designed a structural health monitoring system based on Internet of Things (IoT) and Micro Electro Mechanical Systems (MEMS) sensors. The system has a unique three-layer architecture, including a perception layer for collecting data through MEMS sensors, a network layer for low-power wireless data transmission, and an application layer for cloud based data analysis and visualization. Wavelet transform is also used for signal denoising to reduce external interference. Performance testing shows that the self-made system exhibits excellent performance in bridge vibration monitoring, with time-domain and frequency-domain analysis verifying the accuracy of vibration data. The relative error in frequency identification is only 1.38%. In actual testing, the frequency error of each measuring point is controlled within 3%, and the average relative error is 1.4–1.6%. The research designed building structural health monitoring models have low cost, high accuracy, and reliability, and have broad application prospects in vibration monitoring of building bridges.

**Keywords:** Internet of Things / microelectro mechanical systems / SHM / bridge / building

## 1 Introduction

With the rapid development of urbanization, the number and scale of buildings have increased rapidly. Natural disasters such as earthquakes and storms, as well as long-term wear and tear, can lead to aging or even collapse of building structures [1]. Traditional Structural Health Monitoring (SHM) methods mostly rely on manual inspection, which is inefficient and difficult to achieve real-time monitoring. As the complexity of engineering increases, the demand for construction project layout and optimization also increases [2]. To reduce costs and optimize construction, scholars have conducted extensive research. Fan and Sharma proposed a cost prediction model based on Support Vector Machine (SVM) and least squares method, which utilized preprocessed data for prediction and training, and optimized parameters to improve prediction accuracy [3]. Luong et al. proposed a multi-objective differential evolution algorithm based on adversarial learning to address the trade-off between time, cost, and quality in construction projects. The experiment used highway construction as an example to verify its efficiency and accuracy [4]. Yao et al. designed a

maintenance decision optimization method based on deep reinforcement learning to address the issues of wasted maintenance budgets and poor effectiveness in treating road surface damage. The results indicate that the model can generate optimized maintenance strategies, effectively improve the cost-effectiveness of long-term maintenance, and control road conditions within an acceptable range [5]. To evaluate the design and construction strategies related to the circular economy of new buildings, as well as their application level and readiness. Eberhardt et al. proposed and classified 16 overall architectural design and construction strategies through a systematic literature review. The results show that promoting energy-saving oriented decision-making prioritizes strategies that reduce the impact on the building environment [6]. In response to the high proportion of building energy consumption and carbon emissions, and the difficulty of building thermodynamic models, Yu et al. proposed an intelligent building energy management technology based on deep reinforcement learning. The results show that this method plays an important role in promoting the development of energy-saving and green buildings [7].

To explore the impact of air pollutants in university buildings on indoor air quality and passenger health, Qabbal et al. measured pollutants and comfort factors such as temperature and humidity during three activities using

\* e-mail: [songxianrui@hnjs.edu.cn](mailto:songxianrui@hnjs.edu.cn)

intelligent sensors. The results show that the concentration of CO<sub>2</sub> is as high as 2000 ppm, causing discomfort to residents. 80% of passengers believed that the temperature is uncomfortable [8]. To improve the accuracy and interpretability of the thermal comfort meta model for non-air conditioned buildings, Jaffal combined quasi steady state heat transfer with dynamic simulation results, filtered training data through physical information, and selected appropriate probability distributions to replace polynomials. The results indicate that physics knowledge is more effective than increasing training samples, verifying the flexibility and accuracy of the model [9]. To explore the thermal comfort of building materials, Sawadogo and Coulibaly used KoZiBu software to simulate buildings under reference and optimization conditions. By analyzing the sensitive load, air conditioning load, and temperature curve of a certain building, the thermal environment without air conditioning is studied. The results indicate that adobe materials provide better temperature control and indoor thermal comfort, while also being the most energy-efficient choice, suitable for residential construction in Burkina Faso [10]. Kwong et al. analyzed the distribution of thermal comfort parameters such as air temperature and velocity through electronic sensors, and predicted the temperature and velocity distribution in laboratories and workshops based on fluid dynamics models. Experiments indicate that this model helps optimize the design of air conditioning and mechanical ventilation (ACMV) systems and improve indoor thermal comfort [11]. To improve the stability of light steel structures in super high-rise buildings, Lu et al. calculated the additional internal forces under strong winds based on a stress model and conducted stress analysis. They processed laser scanning data through filtering, defined wind-induced failure criteria, analyzed wind-induced internal pressure and net wind pressure, and used stiffness equations for wind resistance reliability analysis, verifying the efficiency and reliability of the method [12].

In summary, although existing research has shown excellent performance in optimizing construction and improving living environments, there are shortcomings in monitoring the health of building structures, especially in real-time monitoring, damage identification, and structural stress analysis. At present, building structural health monitoring systems both domestically and internationally typically require the installation of a large number of high-precision sensors in the structure, which is costly and has a complex technical architecture. It is also difficult to effectively integrate and share data between different systems. Although some super high-rise buildings have started to establish structural health monitoring systems, overall, the application effect in actual engineering is not ideal, and some systems need to be improved in terms of reliability, accuracy, and other aspects. Microelectro Mechanical Systems (MEMS) have become the core equipment for building health monitoring due to their miniaturization, low power consumption, and high precision [13]. However, the data collected by sensors may contain a significant amount of noise. The denoising method based on Wavelet Transform (WT) has been widely applied in the field of white noise suppression of

partial discharge signals [14,15]. Therefore, to improve the real-time and accuracy of building SHM, this study installed innovative MEMS sensors at key locations and combined with the Internet of Things (IoT) to achieve real-time collection and transmission of data on building structural vibration and stress. WT is applied for signal denoising, and combined with modal parameter identification methods such as random subspace recognition to evaluate the dynamic characteristics of buildings and ensure their structural stability. This study provides an efficient, real-time, and intelligent solution for building SHM, significantly improving monitoring accuracy and reliability.

## 2 Methods and materials

### 2.1 Building structure health monitoring method based on IoT technology

The development of IoT technology has made SHM systems more intelligent and automated. Through sensors, communication technology, and cloud platforms, sensor data can be transmitted, stored, and analyzed in real-time [16]. The SHM system can monitor building performance parameters in real-time, evaluate health conditions, and optimize maintenance and renovation plans based on the evaluation results. In building health monitoring, SHM system achieves data transmission and analysis through IoT technology, which can improve the safety and reliability of building structures. The workflow of the SHM system is shown in Figure 1.

In Figure 1, the workflow of the SHM system is as follows: first, the system obtains monitoring data through data collection, and then performs data analysis. The analysis results are used to determine whether there is damage to the structure. If there is no damage, it will continue monitoring. If damage is found, it will proceed to the next step to locate the location of the damage. Afterwards, it will assess the severity of the injury and further determine the nature of the injury. Based on the evaluation results, the system will take measures to repair or rebuild the structure. The ultimate goal of the entire process is to ensure the health and safety of the structure by evaluating the effectiveness of repairs or reconstructions. The sudden collapse of building structures can be caused by aging, natural disasters, and sudden accidents, and early detection and warning of damage are crucial. However, traditional manual inspections are difficult to perform in real-time. The development of IoT technology makes it possible to automate and monitor building structures over the long term. The building health monitoring system based on the IoT uses intelligent sensors to collect signals, transmit them to cloud servers through the IoT, and store them in a database for management and analysis. Figure 2 shows the three-layer architecture SHM-IoT system framework based on the IoT.

The SHM-IoT system architecture shown in Figure 2 is divided into three main parts: perception layer, network layer, and application layer. The perception layer consists of multiple intelligent sensors that are used to collect health data of physical structures, such as vibration, temperature,

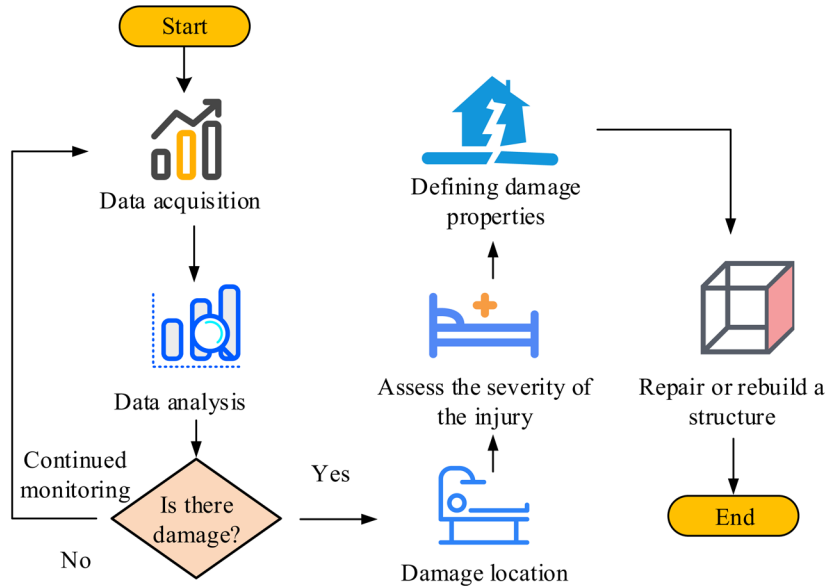


Fig. 1. Workflow of SHM system.

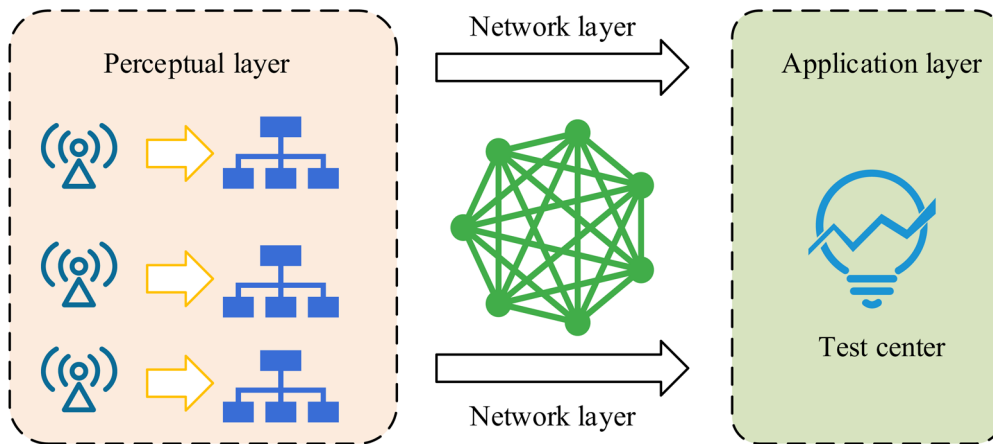
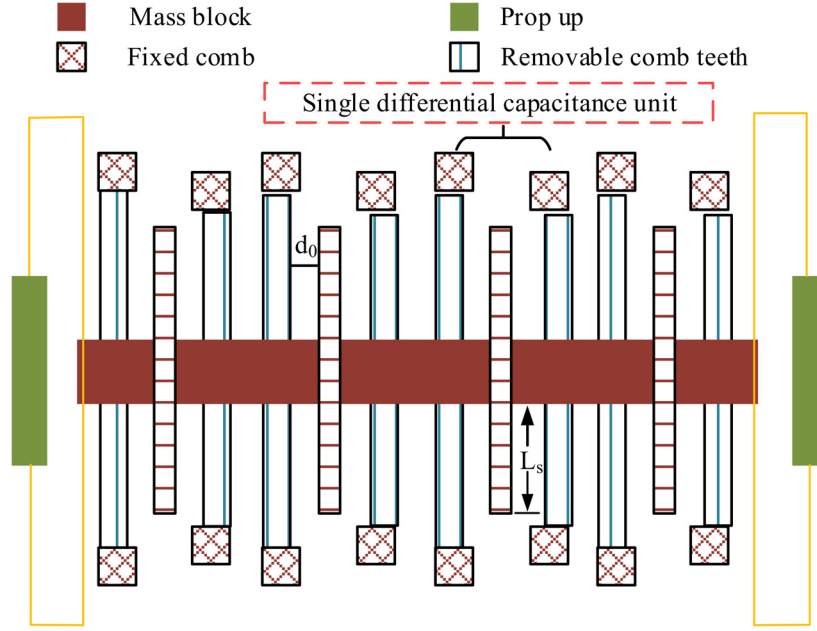


Fig. 2. SHM-IoT system framework based on the three-layer architecture of the IoT.

or stress. Each sensor is equipped with a data preprocessing module to perform preliminary analysis and filtering on the collected raw data, reducing data redundancy and improving data transmission efficiency. The preprocessed data is transmitted through the network layer, which is responsible for connecting various sensor nodes with the monitoring center in the application layer. The monitoring center in the application layer is responsible for receiving and analyzing data from the perception layer, providing real-time monitoring, alerting, and decision support to ensure accurate assessment and management of the structural health status. MEMS is a small integrated device that combines microfabrication technology to integrate electromechanical conversion mechanisms and microcircuits, suitable for signal processing and computing [17]. An accelerometer is one of the most common MEMS devices used to measure the acceleration of an object on different axes. Its internal mechanical components undergo displacement during object acceleration, and these changes are converted into electrical signals by microelectronic

circuits. MEMS accelerometers are classified into piezoelectric, piezoresistive, and capacitive types based on their electrical signal conversion methods [18]. Among them, capacitive sensors have high sensitivity and good stability, making them suitable for low-frequency vibration monitoring and building health monitoring. The structure of the capacitive accelerometer is shown in Figure 3.

The operation of a capacitive accelerometer is based on the movable mass block  $m$ , suspension beam stiffness  $k$ , air damping  $D$ , finger overlap area  $A$ , comb tooth length  $L_s$ , initial sensing gap  $d_0$ , initial capacitance  $C_0$ , and final applied acceleration  $a$ . The suspension beam suspends the mass block, and there are movable comb teeth on both sides of the mass block. When subjected to acceleration, the suspension beam transfers external force to the mass block, causing the gap  $d_0$  between the movable comb teeth and the fixed comb teeth to change, thereby changing the capacitance  $C_1$  and  $C_2$ , while keeping the overlapping area unchanged. The external acceleration is measured based on the change in capacitance. When there is no



**Fig. 3.** Structure of the comb capacitive acceleration sensor.

acceleration  $a=0$ , the left and right capacitors  $C_1$  and  $C_2$  are equal, and the initial capacitance  $C_0$  is as shown in equation (1).

$$C_0 = \frac{\varepsilon_0 \varepsilon_r N_S L_S h}{d_0}. \quad (1)$$

In equation (1),  $\varepsilon_0$  represents the permittivity in vacuum, also known as the electrical constant.  $\varepsilon_r$  stands for relative dielectric constant or dielectric constant.  $N_S$  is the number of plates or layers.  $L_S$  and  $h$  are the length and height of the electrode plates, respectively.  $d_0$  represents the distance between the electrode plates. When the acceleration  $a \neq 0$  exists, the mass block undergoes displacement  $x$  due to acceleration, and the capacitors  $C_1$  and  $C_2$  are functions of  $x$ . The relationship between capacitors  $C_1$  and  $C_2$  can be obtained through equation (2).

$$\begin{cases} C_1 = \frac{\varepsilon_0 \varepsilon_r N_S L_S h}{d_0} \left[1 + \frac{x}{d_0}\right] \\ C_2 = \frac{\varepsilon_0 \varepsilon_r N_S L_S h}{d_0} \left[1 - \frac{x}{d_0}\right] \end{cases}. \quad (2)$$

In equation (2), the variable  $x$  usually represents a certain amount of change. The displacement  $x$  must be very small relative to the gap  $d_0$  between the fixed finger and the movable finger to ensure good linearity. If the capacitance values of  $a \neq 0$ ,  $C_1$  and  $C_2$  are not equal. The capacitance difference can be obtained by measuring this small displacement  $x$ . This difference is represented by equation (3).

$$\Delta C = C_1 - C_2 = \frac{2\varepsilon_0 \varepsilon_r N_S L_S h}{d_0} \left[\frac{x}{d_0}\right] = 2C_0 \left[\frac{x}{d_0}\right]. \quad (3)$$

The capacitance difference between  $C_1$  and  $C_2$  is proportional to the acceleration, which is converted into an electrical signal through microcircuits to obtain the desired

acceleration value. This study used ADXL362 MEMS accelerometer to construct a building structure health monitoring system. ADXL362 is an ultra-low power, 3-axis MEMS accelerometer suitable for high-precision vibration monitoring. The three measurement ranges of  $\pm 2g$ ,  $\pm 4g$ , and  $\pm 8g$  of ADXL362 can meet the needs of different scenarios in building structural health monitoring. When monitoring small vibrations of bridges or buildings, a range of  $\pm 2g$  can be selected to improve measurement accuracy. In scenarios that require significant vibration or impact, a range of  $\pm 8g$  can be selected to prevent exceeding the range. The output data rate of ADXL362 is between 12.5 Hz and 400 Hz, and the bandwidth of its built-in two pole low-pass filter can be set to 1/4 or 1/2 of the output data rate, ensuring effective coverage of the vibration frequency of building structures. Building health monitoring requires processing a large amount of data and has high real-time performance, requiring high communication technology. LTE-Cat1, NB-IoT, and cellular networks are suitable for wide area network transmission. LTE-Cat1 has low power consumption and high speed, making it suitable for real-time data transmission. Compared to traditional 4G networks, LTE-Cat1 has lower equipment and infrastructure costs, better signal coverage, lower latency, and is compatible with existing 4G networks. Therefore, LTE-Cat1 is an effective solution for transmitting building health monitoring data, with advantages such as no need for self-organizing networks, simplified system maintenance, and fast data transmission. In the IoT system, devices or cloud platforms need to constantly communicate with each other, and the communication standard is the protocol. TCP is widely used for building SHM due to its reliability, flow control, and congestion control. It ensures data integrity and sequential transmission through confirmation and retransmission mechanisms, which facilitates time series analysis. In addition, data related to public safety needs to be highly secure, and TCP also provides corresponding security options.

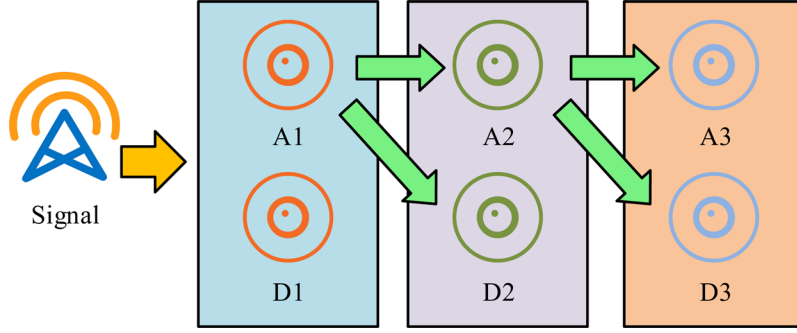


Fig. 4. Structure of three-layer MRA.

## 2.2 Introducing wavelet analysis and MEMS for building structural health monitoring model

However, noise interference often occurs in building SHM. To deal with external interference in vibration signals, such as temperature, humidity, and wind, filtering is usually required. The commonly used filtering methods include low-pass filtering, high pass filtering, median filtering, and wavelet denoising. In practical applications, appropriate filtering methods should be selected based on specific situations, while considering computational complexity and real-time performance. Wavelet Multi-Resolution Analysis (WMRA) uses filters to perform Discrete Wavelet Transform (DWT) techniques, decomposing signals into different resolutions [19]. Coarse resolution contains low-frequency components that preserve the main features of the signal, while fine resolution contains high-frequency components that capture details. By performing scaling operations on wavelets, signal changes at different frequencies can be analyzed. Assuming the scaling parameter is  $m$  and the translation parameter is  $n$ , each  $m$  value corresponds to a different resolution level. The calculation process of the approximation coefficient  $j_{mn}$  for the input signal  $x(i)$  at the  $j$ th resolution is shown in equation (4).

$$j_{m,n} = 2^{(-m/2)} \sum_i x(i) \phi(2^{-m}i - n). \quad (4)$$

In equation (4),  $\phi$  represents the scale function. The calculation process of the approximate signal  $x_m(i)$  at the  $m$ th resolution scale is shown in equation (5).

$$x_m(i) = \sum_{n=-\infty}^{\infty} j_{m,n} \phi_{m,n}(i). \quad (5)$$

The detailed coefficients  $d_{m,n}$  and detailed signals  $g_m(i)$  at the  $m$ th resolution scale are calculated as shown in equation (6).

$$\begin{cases} d_{m,n} = 2^{(-m/2)} \sum_i x(i) \psi(2^{-a}i - n) \\ g_m(i) = \sum_{k=-\infty}^{\infty} d_{m,n} \cdot \psi_{m,n}(i) \end{cases}. \quad (6)$$

In equation (6),  $\psi_{m,n}(i)$  represents the wavelet basis function. The above three steps are repeated for the resolution scale of  $a+1$ . By using the approximate  $x_m(i)$

obtained in equation (6), the original signal  $x(i)$  can be decomposed at an infinite resolution level according to the formula and reconstructed using the obtained infinite details, as shown in equation (7).

$$x(i) = \sum_{m=-\infty}^{\infty} g_j(i) = \sum_{m=-\infty}^{\infty} \sum_{n=-\infty}^{\infty} d_{m,n} \psi_{m,n}(i). \quad (7)$$

The above content describes the multi-resolution analysis (MRA) of stop signals at M-level resolution in practical applications. The signal is approximately reconstructed through M-level resolution, while obtaining all details from the first level to M-level. The formula illustrates this process as shown in equation (8).

$$x(i) = \sum_{n=-\infty}^{\infty} j_{M,n} \cdot \phi_{M,n}(i) + \sum_{m=1}^M \sum_{n=-\infty}^{\infty} d_{m,n} \cdot \psi_{m,n}(i). \quad (8)$$

The first term represents M-level approximation, while the second term represents M-level and below details. MRA adopts a pyramid structure, and through iterative application of scale functions and wavelet functions, the WRA structure is shown in Figure 4. The high-frequency outputs are coefficients (D1, D2, D3), and the low-frequency outputs are approximate coefficients (A1, A2, A3). It should be noted that MRA mainly decomposes the low-frequency part to save computation time and storage resources, while high-low frequency decomposition is considered in wavelet packet analysis.

Wavelet analysis has been applied in signal denoising due to its localization, time-frequency domain analysis, and MRA characteristics. The commonly used wavelet threshold denoising method utilizes the characteristics of signals and noise at different scales, and achieves precise processing through MRA [20]. The specific steps for denoising are shown in Figure 5.

In Figure 5, to remove noise from the signal, the system first performs WT on the signal and selects appropriate wavelet basis functions and decomposition levels. This step decomposes the signal into sub signals of different scales and can be processed using either hard thresholding or soft thresholding methods. Hard thresholding sets coefficients smaller than the threshold to zero, while soft thresholding compresses these coefficients. Based on the characteristics of noise, fixed or adaptive thresholds can be selected to enhance the denoising effect. After thresholding, the

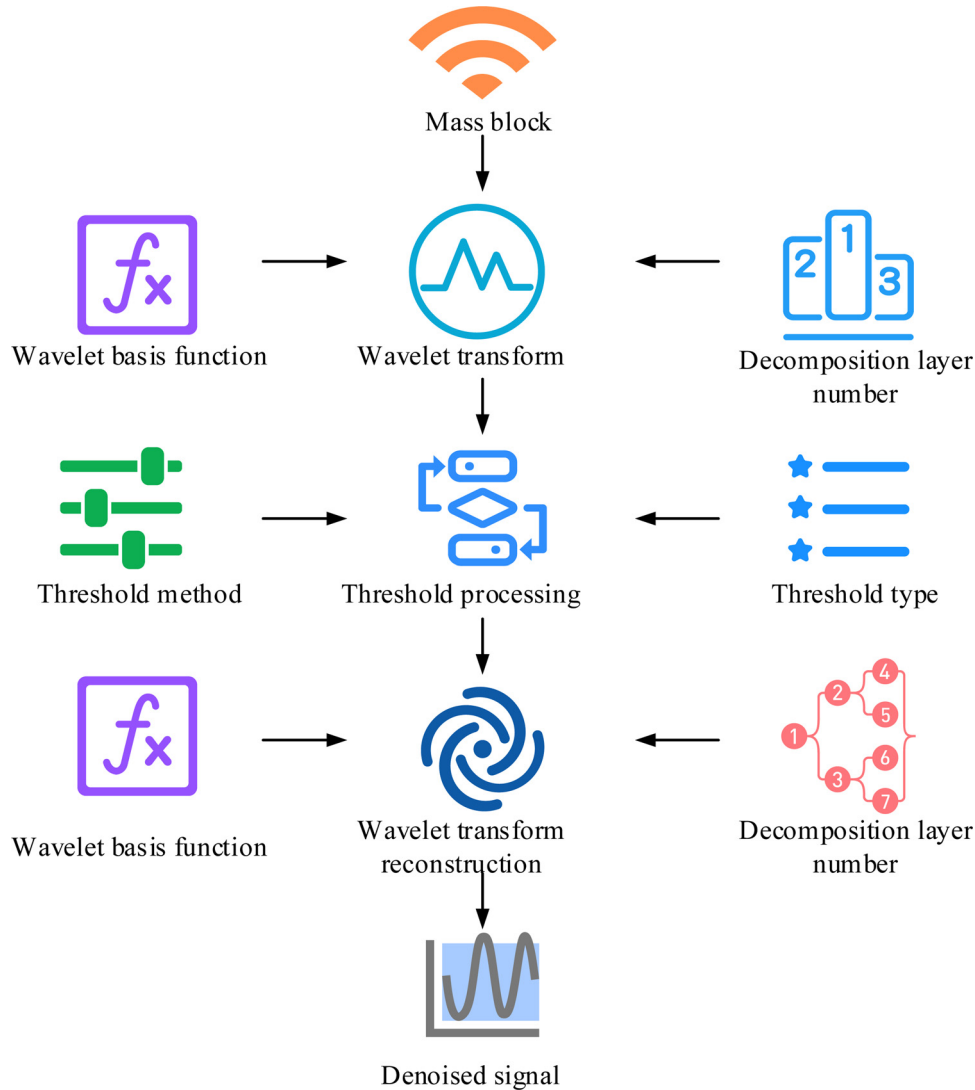


Fig. 5. Basic flow of wavelet threshold denoising.

processed wavelet coefficients are transformed back into time-domain signals using wavelet inverse transform, resulting in denoised signals. The main function of the SHM system is to collect, process, and analyze data through sensors installed on the structure in order to identify and locate structural damage, evaluate structural condition, and predict remaining life. By analyzing the vibration data, modal parameters of the structure can be obtained to detect and identify the degree and location of damage, and evaluate its impact on structural integrity. Vibration measurement mainly relies on the implementation of monitoring terminals. The design of SHM system based on the IoT involves the software and hardware design of monitoring terminals and the development of cloud platforms. The building SHM model is shown in Figure 6.

In Figure 6, the building SHM system based on the IoT includes three parts: monitoring terminals, base stations, and cloud platforms. The monitoring terminal consists of a main control module, communication module, power

supply module, and acceleration sensor, responsible for data acquisition, processing, and uploading. The optimized main control module can use high-performance processors or edge computing to reduce data transmission. The communication module should choose appropriate protocols based on specific situations, such as LoRa and 5G. Sensors can be combined with multiple types of sensors to improve data accuracy. It is recommended to set up a backup or use energy harvesting technology for the power supply module to ensure continuous power supply. The base station is responsible for data reception and upload, with redundant design and signal optimization to improve data transmission quality. The cloud platform performs data storage and processing to support user queries, analysis and visualization. To reduce transmission delay, the system can use data compression, edge computing and appropriate protocols to design a failure recovery mechanism and conduct energy consumption assessment to extend the system life.

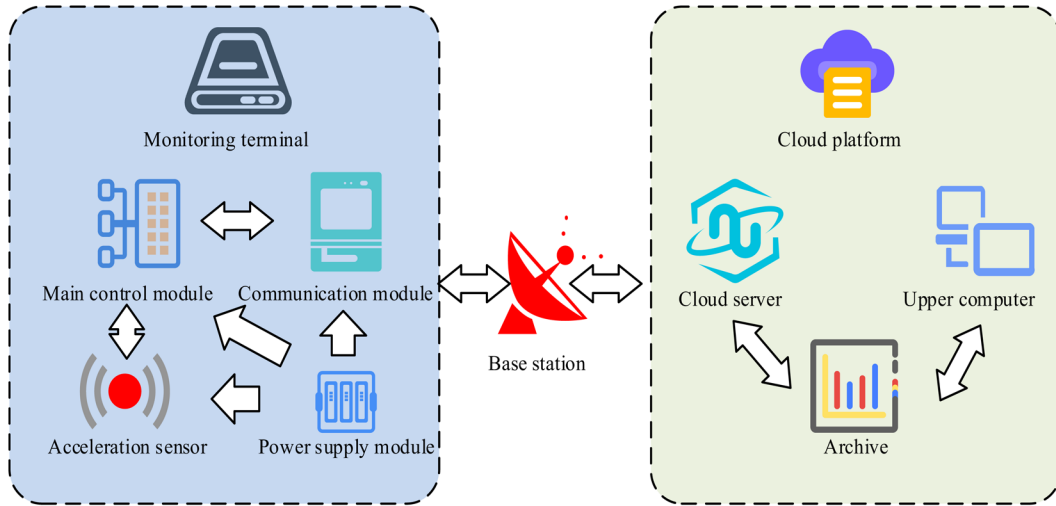


Fig. 6. Building SHM model.

Table 1. Performance parameters of ADXL362 MEMS sensor.

Parameter name	Parameter index	Parameter name	Parameter index
Acceleration range	$\pm 2g, \pm 4g, \pm 8g$	Output resolution	12bit
Nonlinearity	$\pm 0.5\%$	Supply voltage range	1.6–3.5V
Operating temperature range	$-40\sim+85^{\circ}\text{C}$	Overall module size	3 mm $\times$ 3.25 mm $\times$ 1.06 mm
Output rate	12.5~400Hz	Deep multi-mode output	FIFO

### 3 Results

The experimental bridge is a simply supported steel beam bridge with a span of 9.6 m and a width of 2.4 m. The main beam of the bridge is made of IPE300 I-beam, and the bridge deck pavement is made of 100 mm thick C30 concrete. The bridge adopts simply supported bearings at both ends, with a spacing of 9.6 m between the bearings. The design load of the bridge is highway level II, and it can withstand a maximum uniformly distributed load of 8.5 kPa. The experiment used multi-point acceleration sensors arranged with a sensor range set to  $\pm 2G$  and a sampling frequency of 100Hz. To accurately collect vibration signals, sensors were arranged at the midpoint of the bridge span and at the 1/4 and 3/4 positions of the span. The experiment stimulated bridge structures through jumping, which can be divided into two methods: single jump and continuous jump. The test data was collected through a self-made monitoring system and compared with data from commercial equipment to verify its reliability. The finite element modeling adopted Ansys software to simulate the modal analysis of the bridge to obtain the natural frequencies and vibration modes. Table 1 shows the detailed performance parameters of the ADXL362 accelerometer used in the study.

The research model consists of data processing, data analysis, modal analysis, and parameter setting. First was to import the acceleration data from the monitoring points and generate an auxiliary acceleration time history chart. The modal analysis module calculated the principal

frequencies, damping ratios, and principal mode vectors of each order using the SSI-COV method. The parameter setting module was used to adjust parameters such as sampling frequency and filtering layers. The cost comparison between the self-made monitoring system and the commercial system is shown in Figure 7.

In Figure 7, there was a significant difference in cost between self-made monitoring systems and commercial monitoring systems. The prices of commercial sensors, filters, and data acquisition cards were 700 yuan, 1050 yuan, and 2000 yuan, respectively, while the costs of ADXL362 sensors, core boards, and communication modules used in self-made systems were 15 yuan, 156 yuan, and 50 yuan, respectively. In addition, the self-made system also used solar panels and batteries, with a cost of 281 yuan. Overall, the cost of homemade monitoring systems was much lower than that of commercial systems, especially in the sensor and data acquisition parts. To verify the performance and reliability of the accelerometer system, experiments were conducted on a steel structure glass pedestrian bridge model and a pedestrian overpass in Zhengzhou. The bridge model adopted I22a steel main beam and double-layer laminated tempered glass bridge deck, with a width of 1.2m and a net span of 11.8m. The comparison devices were INV3062T data acquisition analyzer and DH610 electromagnetic vibration sensor, which are suitable for low-frequency vibration measurement. The vibration of the bridge body was stimulated by personnel walking, and the vertical acceleration time-domain test results are shown in Figure 8.

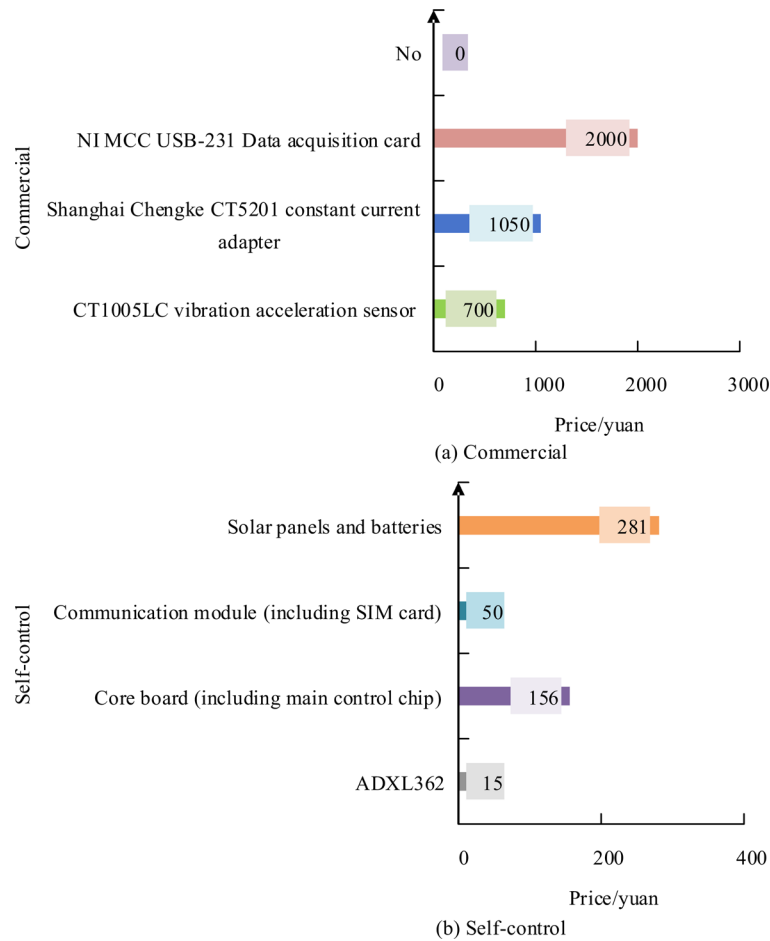


Fig. 7. Cost comparison between self-made monitoring system and commercial system.

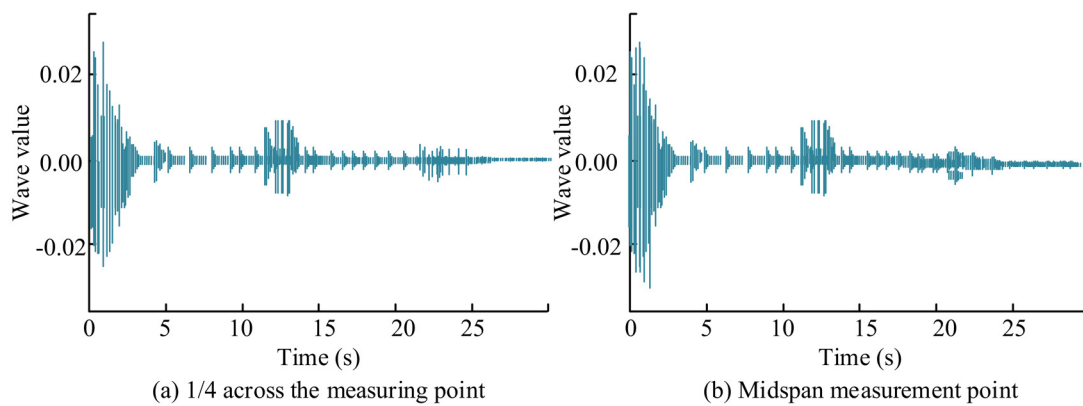


Fig. 8. Time-domain diagram of vertical acceleration.

In Figure 8a, the amplitude of the 1/4 span measurement point is relatively large within 0–4s, and over time, the vibration amplitude gradually decreased, exhibiting a typical trend of free vibration attenuation. The vibration rapidly decayed within 10 seconds and gradually stabilized thereafter. The time-domain plot of the mid span measurement point in Figure 8b showed a similar attenuation trend, but with a slightly larger initial amplitude fluctuating between  $\pm 0.03$  g and a longer

attenuation time. Overall, the vibration amplitude and duration at the mid span position were slightly greater than those at 1/4 of the span measurement point. This indicates that the vibration impact on the mid span position is more significant, with more vibration energy, while the 1/4 span position is relatively smaller. The shaking of vertical acceleration is due to the fact that the experiment simulates the vibration excitation of the bridge through jumping, which may have temporal uncertainty and

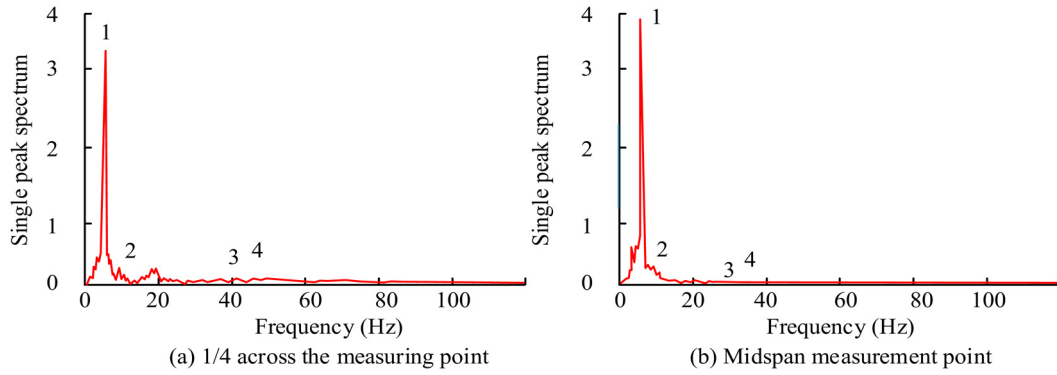


Fig. 9. Frequency domain diagram of vertical acceleration.

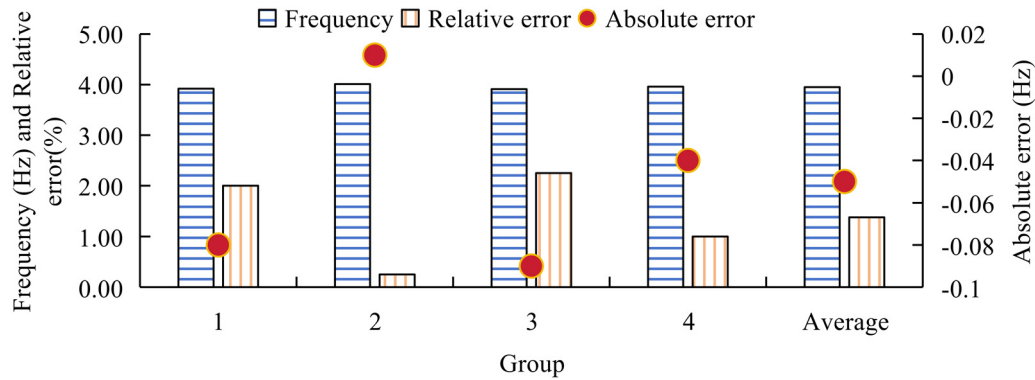


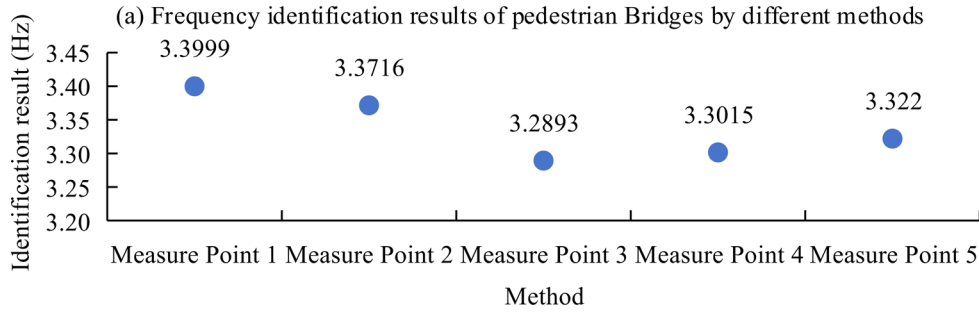
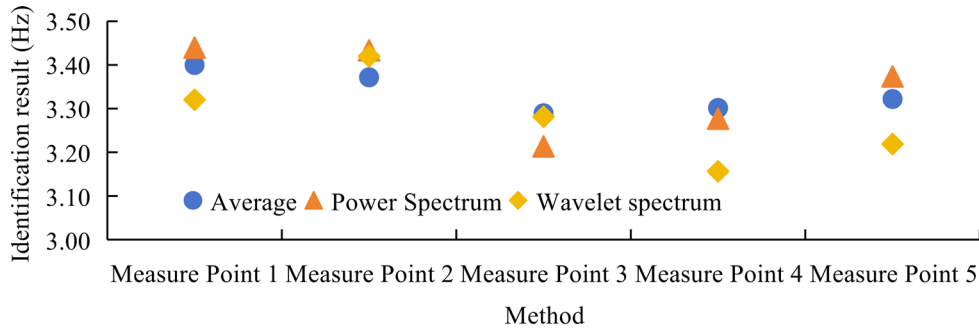
Fig. 10. Relative error results of frequency identification.

intensity changes, resulting in sudden shaking of the signal recorded by the accelerometer. Figure 9 shows the frequency domain diagram of vertical acceleration.

From the frequency spectrum of the 1/4 span measurement point in Figure 9a, the main frequency of the vibration was about 4.2 Hz, with a significant peak, indicating that this frequency was the main mode of the structure. In addition, some small amplitude vibration peaks also appeared at 2 Hz and 35.8 Hz, indicating that these frequencies may be secondary modes. The spectrum of the mid span measurement point in Figure 9b showed that the main frequency was also 4.2 Hz, but its peak amplitude was larger and the vibration was more significant. At the same time, secondary frequency peaks were also detected at 2 Hz, 34 Hz, and 35.8 Hz, consistent with the results of the 1/4 cross measurement point. From the frequency domain results of these two measurement points, the vibration of the bridge was most pronounced at 4.2 Hz, which belongs to the primary modal frequency, while other secondary modal frequencies also had an impact on the overall vibration characteristics of the bridge structure. In the vibration measurement experiment of the steel structure glass pedestrian bridge model, sensor arrangements were used at mid span (measurement point 1), 1/4 span, and 3/4 span (measurement points 2 and 3, respectively). Due to the width of the bridge deck being only 1 meter, the sensor was placed on the centerline of the bridge deck, making it effective and convenient to deploy. Using the jumping of experimental personnel on the

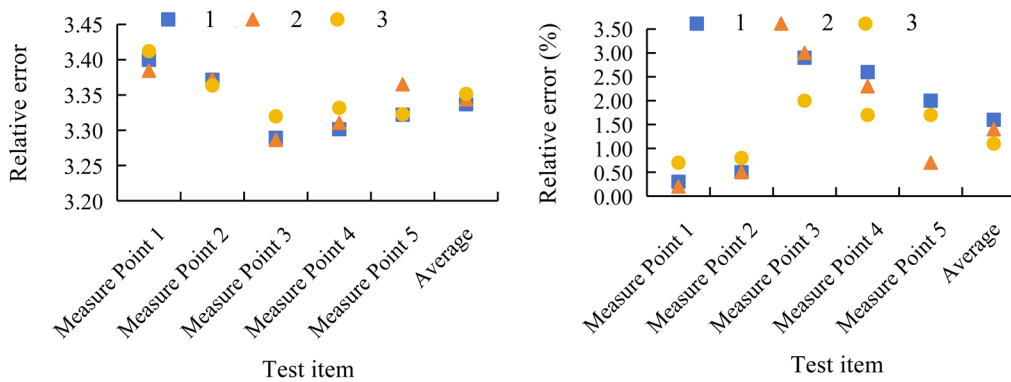
bridge deck as motivation, they were divided into two groups: single jump and multiple consecutive jumps. A single jump is an instantaneous impact with high intensity. Multiple jumps result in longer duration and higher frequency. The experimental data was obtained through a cloud server and subjected to wavelet denoising using Matlab. The sym4 wavelet was selected and subjected to 3-level decomposition, soft thresholding, followed by FFT transformation, power spectrum analysis, and wavelet spectrum analysis. The relative error of frequency recognition is shown in Figure 10.

In Figure 10, the self-made monitoring system had a smaller frequency recognition error compared to commercial equipment. The four experimental frequencies were 3.92 Hz, 4.01 Hz, 3.91 Hz, and 3.96 Hz, with an average of 3.95 Hz, which was only 0.05 Hz lower than the commercial equipment's 4 Hz, indicating a relatively low error. The maximum absolute error was 0.08 Hz and the relative error was 2%. The minimum absolute error was 0.01 Hz and the relative error was 0.25%. The average relative error was 1.38%, indicating that the self-made system had high accuracy and could effectively identify the natural frequency of the structure. After the performance verification of the self-made building structure health monitoring system, on-site dynamic characteristic tests were conducted on a pedestrian overpass in Zhengzhou city, focusing on modal parameters such as minimum natural frequency, mode shape, and damping ratio. By arranging five accelerometers in the bridge, the data was recorded at a

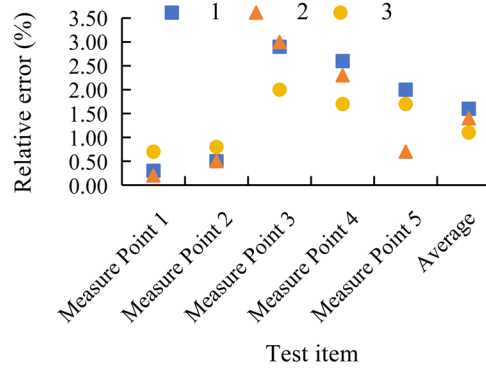


(b) The average of pedestrian bridge frequency identification results at each measuring point

**Fig. 11.** Frequency identification results of pedestrian Bridges with different methods.



(a) The relative error value of the frequency identification results of construction Bridges



(b) Relative error ratio of frequency identification results of construction Bridges

**Fig. 12.** Relative error of pedestrian bridge frequency identification results.

sampling frequency of 100 Hz. The selection of measuring points was based on the optimal quantity, optimal positioning, and clear experimental objectives. The frequency recognition results of different methods are shown in Figure 11.

In Figure 11, three methods including FFT, power spectrum, and wavelet spectrum were used to analyze the frequencies of different measurement points on the pedestrian overpass. The results showed that the frequency recognition values of the three methods were similar but slightly different. Overall, the frequencies of measurement points 2 and 4 were higher, while measurement point 3 was lower. The frequency fluctuations of each measuring point were small, reflecting the consistency of the dynamic characteristics of the bridge structure, indicating that the

frequency distribution was uniform and the overall structural stability was good. The accelerometer could accurately and effectively identify the fundamental natural frequency of the pedestrian bridge, which was approximately 3.34 Hz. To ensure the reliability of the experiment, the monitoring system was set to be triggered by RTC timing with an interval of 1 h, and two data collections were conducted. The results are shown in Figure 12.

From Figure 12, the frequency recognition results of the five measurement points had relatively small errors, and the errors of all measurement points were controlled within 3%, with an average relative error of 1.4% to 1.6%. Among them, the error of measuring point 3 was generally large, especially in tests of measuring points 1 and 2 where the error reached nearly 3%. Overall, the frequency identification

values of each measuring point were relatively consistent, indicating that the structural dynamic characteristics of pedestrian overpasses had good stability and consistency. The data analysis further proved the uniformity of the frequency distribution of the bridge, and the frequency identification error of the bridge structure at different positions fluctuated less, verifying the reliability of the experimental method.

## 4 Discussion and conclusion

It is crucial to accurately identify the natural frequency of a bridge to evaluate its structural health status. Based on IoT technology, research used methods such as fast Fourier transform, power spectrum analysis, and wavelet analysis to identify the frequency of different measuring points on pedestrian overpasses. MEMS acceleration sensors were used to collect data and analyze the frequency distribution of each measuring point. Cost comparison showed that self-made monitoring systems outperformed commercial systems in terms of cost and performance. Time-domain analysis showed that the amplitude and duration of the mid span measurement point were both greater than 1/4 of the span measurement point, reflecting the characteristics of vibration energy distribution. Frequency domain analysis showed that the main frequency of 4.2 Hz was consistent with the secondary modal frequencies (such as 2 Hz and 35.8 Hz), indicating that the system could accurately identify modal frequencies. The experimental results verified the high accuracy of the self-made system, with a relative error of only 1.38% in frequency recognition. In actual bridge testing, the frequency error of different measuring points was controlled within 3%, and the average relative error was 1.4% to 1.6%, reflecting the dynamic stability of the bridge structure. In summary, the proposed building structure health monitoring model system has demonstrated certain advantages in bridge vibration monitoring, with low cost, high accuracy, and good reliability. However, due to factors such as mechanical stress release, temperature changes, and electronic component aging inside the sensor, MEMS sensors have long-term drift problems, which may lead to zero drift and sensitivity changes in the sensor, thereby affecting the accuracy and reliability of monitoring data. Therefore, future research should further establish a regular sensor calibration mechanism, using standard vibration tables or reference signals to calibrate sensors to compensate for their long-term drift.

### Funding

No funding.

### Conflicts interests

The author reports there is no conflict interests.

### Data availability statement

The data are provided within the manuscript.

### Author contribution statement

The manuscript was independently written by the author Xianrui Song, who made great contributions to the manuscript.

### References

1. N. Maloth, K. Vimal, P. Joy, A convolutional neural network-based architecture for health monitoring of joint damages in a steel plane frame structure under temperature variability, *Asian. J. Civ. Eng. Build. Hous.* **25**, 2077–2090 (2024)
2. A.M. Usman, M.K. Abdullah, An assessment of building energy consumption characteristics using analytical energy and carbon footprint assessment model, *Green Low-Carbon Econ.* **1**, 28–40 (2023)
3. M. Fan, A. Sharma, Design and implementation of construction cost prediction model based on SVM and LSSVM in industries 4.0, *Int. J. Intell. Comput. Cybern.* **14**, 145–157 (2021)
4. D.L. Luong, D.H. Tran, P.T. Nguyen, Optimizing multi-mode time-cost-quality trade-off of construction project using opposition multiple objective difference evolution, *Int. J. Constr. Manage.* **21**, 271–283 (2021)
5. L. Yao, Q. Dong, J. Jiang, F. Ni, Deep reinforcement learning for long-term pavement maintenance planning, *Comput. –Aided Civ. Infrastruct. Eng.* **35**, 1230–1245 (2020)
6. L.C.M. Eberhardt, M. Birkved, H. Birgisdottir, Building design and construction strategies for a circular economy, *Archit. Eng. Des. Manag.* **18**, 93–113 (2022)
7. L. Yu, S. Qin, M. Zhang, C. Shen, T. Jiang, X. Guan, A review of deep reinforcement learning for smart building energy management, *IEEE Internet Things J.* **8**, 12046–12063 (2021)
8. L. Qabbal, Z. Younsi, H. Naji, An indoor air quality and thermal comfort appraisal in a retrofitted university building via low-cost smart sensor, *Indoor Built Environ.* **31**, 586–606 (2022)
9. I. Jaffal, Physics-informed machine learning for metamodeling thermal comfort in non-air-conditioned buildings, *Build. Simul.* **16** 299–316 (2023)
10. D. Sawadogo, O. Coulibaly, Comparative study of the thermal comfort of four materials type used in the construction of a building, *J. Energy Power Eng.* **15**, 231–242 (2021)
11. Q.J. Kwong, J.Y. Yang, O.H.L. Ling, O.H.L. Ling, R. Edwards, J. Abdullah, Thermal comfort prediction of air-conditioned and passively cooled engineering testing centres in a higher educational institution using CFD, *Smart Sustain. Built Environ.* **10**, 18–36 (2021)
12. C. Lu, Z. Yang, L. Zheng, Z. Liu, Smart reliability analysis of wind resistance of lightweight steel structures in super tall buildings in a smart city, *J. Test. Eval.* **51**, 1793–1803 (2023)
13. L. Zhou, F. Kato, M. Iijima, Mass-fabrication scheme of highly sensitive wireless electrodeless MEMS QCM biosensor with antennas on inner walls of microchannel, *Anal. Chem.* **95**, 5507–5513 (2023)
14. P. Biglarbeigi, A. Morelli, S. Pauly, Unraveling spatiotemporal transient dynamics at the nanoscale via wavelet transform-based Kelvin probe force microscopy, *ACS Nano.* **17**, 21506–21517 (2023)
15. H.U. Yaokun, T. Toda, The effect of multi-directional on remote heart rate measurement using PA-LI joint ICE-EMDAN method with mm-wave FMCW radar, *IEICE Trans. Commun.* E105.B, 159–167 (2022)

16. D. Marques, D. Vandepitte, V. Tita, Sensitivity and uncertainty analysis for structural health monitoring with crack propagation under random loads: A numerical framework in the frequency domain, *Fatigue Fract. Eng. Mater. Struct.* **46**, 137–152 (2023)
17. T. Serdar, A. Metin, Integration of conducting polymers with MEMS lateral comb-drive resonator via electrodeposition for VOCs detection, *J. Mater. Sci.* **58**, 3078–3093 (2023)
18. M.W. Pruessner, N.F. Tyndall, T.H. Stievater, MEMS-tunable polarization management in photonic integrated circuits, *Opt Express.* **31**, 31316–31328 (2023)
19. A.N. Pavlov, O.N. Pavlova, O.V. Semyachkina-Glushkovskaya et al. Enhanced multiresolution wavelet analysis of complex dynamics in nonlinear systems, *Chaos.* **31**, 1–9 (2021)
20. G. Zhu, B. Liu, P. Yang, X. Fan, Image denoising method based on improved wavelet threshold algorithm, *Multimedia Tools Appl.* **83**, 67997–68011 (2024)

**Cite this article as:** X. Song: Design of building structure health monitoring model based on IoT and MEMS sensors. *Sust. Build.* **8**, 4 (2025). <https://doi.org/10.1051/sbuild/2025008>